Desalination and Water Treatment
www.deswater.com
doi: 10.5004/dwt.2018.22569

128 (2018) 11–19
October

The evaluation of 3D morphological structure of porous membranes based on a computer-aided analysis of their 2D images

Małgorzata Przytulska*, Juliusz Lech Kulikowski, Monika Wasyłeczko, Andrzej Chwojnowski, Dariusz Piętka

Nałęcz Institute of Biocybernetic and Biomedical Engineering, Trojdena 4 Street, 02-109 Warszawa, Poland, Tel. +48 22 5925950; Fax: +48 22 6597030; emails: mprzytulska@ibib.waw.pl (M. Przytulska), jkulikowski@ibib.waw.pl (J.L. Kulikowski), mwasyleczko@ibib.waw.pl (M. Wasyłeczko), achwojnowski@ibib.waw.pl (A. Chwojnowski), bpietka@ibib.waw.pl (D. Piętka)

Received 2 February 2018; Accepted 26 March 2018

ABSTRACT

A method of a computer-aided analysis and a description of three-dimensional (3D) morphological structure of porous membranes based on two-dimensional images of cross-sections of a material is presented in the paper. The parameters of pores' shape factor regularity are defined. Theoretical backgrounds of regular pores analysis based on a statistical approach are presented. The method was implemented in a computer program MeMoExplorer™, which is also shortly described in the paper. Results of application of the method for analysis of a series of electron microscope images of cross-sections of samples of polyethersulfone membranes are presented. Suggestions concerning possible extension of 3D analysis of morphological structure on irregularly shaped pores in the concluding section are given.

Keywords: Porous membranes; Three-dimensional porosity analysis; Computer-aided image processing

1. Introduction

Porous materials in the form of membranes and/or scaffolds play a substantial role in various areas of technology and biomedical applications [1–4]. In particular, they can be used in biological tissue engineering as a support for biological cells cultivation and forming artificial organs [5–8]. In this case, they should meet some specific requirements which roughly can be divided into several groups: physical, mechanical, biochemical, etc. [9–12]. Physical requirements concern permeability of a porous material for selected types of particles, a susceptibility of inner surface of pores to biological cells adhesion and seeding, heat conductivity, etc. A mechanical strength and an elasticity represent the next group of requirements. The third group covers the requirements on the absence of harmful biochemical reactions between the material and the cells, controlled biodegradability of the material, while the process of cells colony growth is in progress, etc. These requirements thus should be estimated and carefully controlled during the process of porous material production.

Physical properties of porous materials are directly influenced by their micromorphological structure [13–19]. The size and the shape of pores should provide a microenvironment for cells migration and seeding. In addition, small pores in the walls of membranes should facilitate cells nutrition and removal of the metabolic waste products. Hence, a quantitative evaluation of a morphological structure plays a substantial role in porous materials production as well as in their technological or biomedical applications. For this purpose, samples of porous materials are cut into cross-sections subjected to microscopic examinations. Pores visible in the specimens can be parameterized and classified according to their size and shape by using computer techniques. In a former publication [20] on this topic, a method of the

* Corresponding author.

Presented at the XII Scientific Conference "Membranes and Membrane Processes in Environmental Protection" – MEMPEP 2018 13–16 June 2018, Zakopane, Poland.

quality of polyethersulfone (BASF) membranes assessment based on computer-aided image analysis was described. The porosity characteristics were based there on the statistics of automatically measured areas of cross-sections of segmented (selected and contoured) pores. However, it was clear that some physical properties, like for example, permeability of porous materials, depended on three-dimensional (3D) rather than on two-dimensional (2D) morphological structure of the material. Unfortunately, the fragility of the analyzed materials makes cutting several parallel slices from any given sample of the material impossible. Therefore, the set of measurable parameters is limited to those concerning a single 2D section of any sample. On the other hand, a 3D morphological structure of pores in individual samples of a material is of a great interest. The aim of this paper consists thus in *explaining which information concerning the morphological 3D structure of pores, substantial for a membranes quality assessment, can be extracted by computer-aided analysis of 2D images of cross-sections of membranes*.

Two approaches to explain this issue are presented as follows: (1) statistical extension of the results of 2D image analysis on the third dimension and (2) analysis of the histograms of the brightness level within the areas of segmented pores. The first approach is not quite new, in medical cardio-diagnosis the 3D-volume of some inner organs is roughly evaluated on the basis of their 2D imaging in X-ray or ultrasound modalities [21,22]. Such approach is admissible at the assumption of convexity and sufficient regularity of the form of examined objects. However, in the case of some types of porous membranes this assumption is not quite valid, the pores may arise as irregular cavities surrounding squeezed fibrous material and none of the known geometrical objects can be used as a satisfactory model of their shape. In such case, an alternative approach to membranes porosity evaluation, based on combined morphological and statistical deep analysis of 2D images, but without the use of the concept of exactly segmented pores, is proposed.

2. Materials

Samples of membranes obtained by dry–wet phase inversion method [23,24] from a mixture of copoli-l-lactide-glycolide (Corbion) and BASF using dioxan-1.4 (POCh) as a solvent were analyzed. In another series of experiments solutions of Corbion in dichloromethane (POCh) and BASF in *N*-methyl-pyrrolidone (MERCK KGaA, Darmstadt, Germany) were used. This gave several types of produced membranes to be examined. The samples of so-obtained materials were cut, covered by 7–10 nm thick gold layers (K550X Emitech Sputter Coater), and so-prepared cross-sections were visualized in 300 × and 1,000 × magnification by scanning electron microscope (SEM) Hitachi TM1000. The series of images presenting the cross-sections of various types of membranes then were subjected to more advanced computer analysis.

Figs. 1(a)–(c) illustrate the variety of shapes and sizes of pores visible in the cross-sections of membranes (all images are presented in the same 1,000× magnification): from the pores of quasi-ellipsoidal shape (a) through the areas surrounding moderately irregular fibrous structures (b) up to the areas surrounding highly irregular quasi-fibrous structures (c).

The images were provided for analysis of 10 series, containing from 6 to 21 images, each series representing a selected type of a membrane. An exemplary series of images representing an Ig-PVP (polyvinylpyrrolidone) type porous material (obtained by the use of fibrous gel as a precursor of pores and polyvinylpyrrolidone added as a component of the solving medium [23,24]) are shown in Fig. 2.

3. Methods

3.1. Theoretical backgrounds

Pores can be defined as holes disseminated and penetrating solid materials. A porosity, in general, is an important (sometimes – positive, sometimes – undesired) property of a material. However, the notion of *porosity* needs to be more strictly defined, because, as shown in Fig. 1, it can be referred to the pores of a various density, size, and/or form. It seems thus reasonable to characterize porosity by several measurable parameters selected adequately to the given application area. Theoretically, the following strictly defined parameters could be taken into consideration in a first step:

- Pores density:

$$g = \frac{\text{total volume } V_p \text{ of pores in a sample of material}}{\text{total volume } V_{\text{tot}} \text{ of the sample}} \quad (1)$$

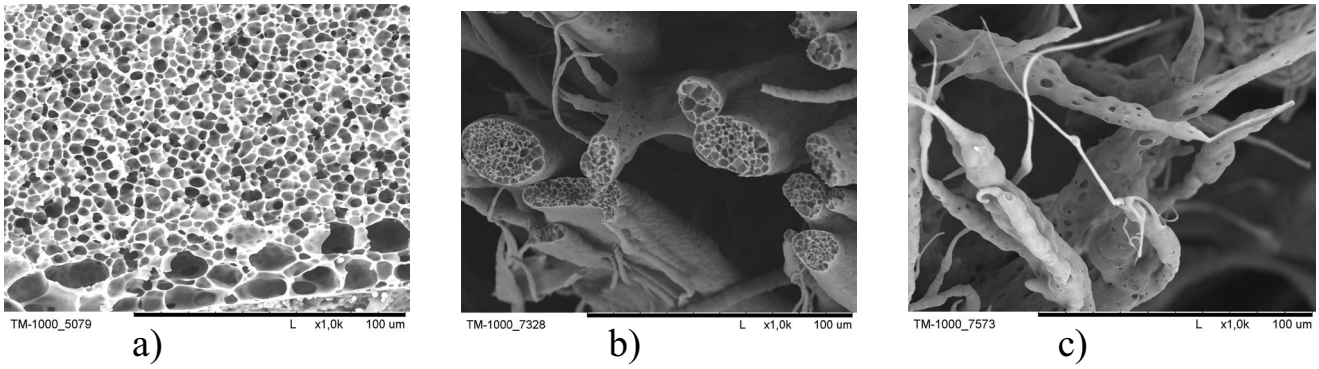

Fig. 1. Various types of pores forms: (a) quasi-ellipsoidal, (b) interfiber moderately irregular, (c) interfiber highly irregular. 1,000× magnification.

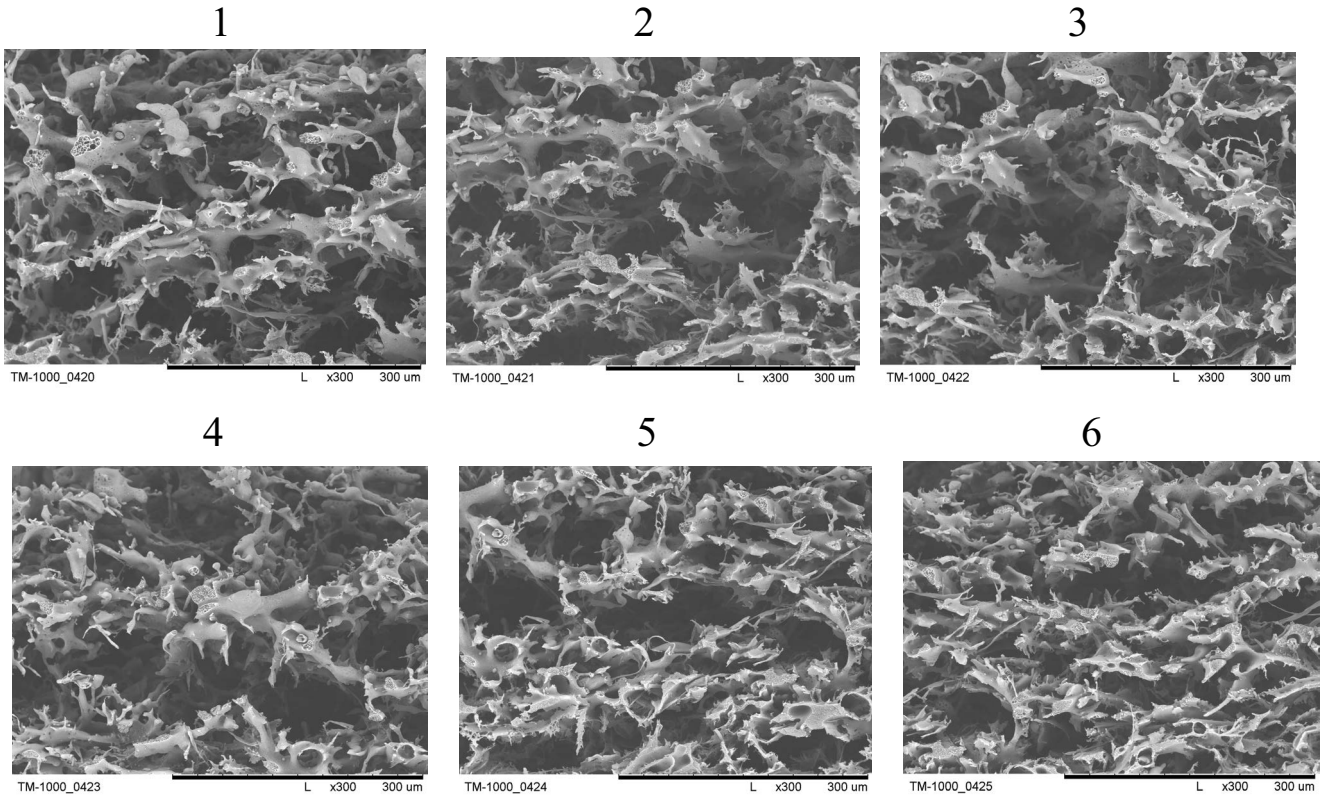

Fig. 2. A series of SEM-images of Ig-PVP (polyvinylpyrrolidone)-type porous material cross-sections. (The abbreviation MWCk is only a membranes mark. It is not chemically relevant.)

- Histogram H of volumes V of pores, their mean value V_{mean}, standard deviation V_{std} and, if necessary, higher-level statistical moments;
- Shape factor f of pore given by the (one of several possible) formula:

$$f = \frac{S^{3/2}}{6\sqrt{\pi}V} \cong 0.094\frac{S^{3/2}}{V} \tag{2}$$

where S denotes the inner surface area of a pore and V, the pore's volume. The shape factor f is equal to 1 for a spherical pore and increases unlimitedly in other shapes (e.g., $f \cong 1.382$ in cubes). Therefore, f seems to be suitable to be used as a characteristic of pores shape *regularity*. Unfortunately, this cannot be exactly done exactly, because the input data S and V in 2D images of cross-sections of pores are directly inaccessible. A solution of this problem, based on the following assumptions, is thus proposed:

- Assumption 1

The size and shapes of pores are random variables, statistical characteristics of which are specific for a given type of porous materials.

- Assumption 2

In isotropic materials, statistical characteristics are independent of a spatial orientation of 1D (linear) or 2D (planar) cross-section of a sample of the material.

- Assumption 3

The higher is the regularity of pores shape the higher may be the accuracy of 3D porosity characteristics evaluation based on the analysis of 1D or 2D measurable parameters.

In particular, the shape factor f can be substituted by the following 2D *shape factor* R_s of a contoured pore's section:

$$R_s = \frac{l_s^2}{4\pi S_s} \tag{3}$$

where l_s denotes the *length* (*perimeter*) *of contour* and S_s, the area of the cross-section of a pore. Both parameters in the 2D image can be relatively easily measured [20]. The shape factor R_s is equal to 1 for circular contours and increases unlimitedly for other shapes (e.g., $R_s \cong 1.273$ for squares).

On the basis of R_s all segmented and contoured pores in a 2D image can be preliminarily divided into two classes:

- *regular*, if $1 \le R_s < R^*$,
- *irregular*, if $R_s > R^*$,

where $R^* > 1$ is an arbitrarily selected *regularity level* of pores' cross-sections.

If *regular* pores (e.g., by fixed $R^* = 1.1$) are the dominant ones in the 2D image then they can be processed like if they represent almost spherical shapes. However, it does not mean that radii r_s of visible pores sections can be identified with the real radii r of pores. A regular spherical pore can be

cut by a plane on various distances δ to the sphere center *O* and the observable radius r_s of a pore's cross-section depends on δ as shown in Fig. 3.

The analysis of regular pores sections (like those shown in Fig. 1(a)) may provide only the radii r_s and their histogram $h(r_s)$ approximating the (a priori unknown) *probability density function* (*pdf*) $u(r_s)$. Further considerations are based on:

- Assumption 4

The sphere can be cut (symmetrically, in the upper or lower hemisphere) at distance δ to the center *O* *equally distributed* in the interval [0,*r*] (and, similarly, in the lower hemisphere).

If one normalizes all distances under consideration by dividing them by *r*; all so-normalized distance-values are below underlined. Then $\underline{r} = 1$ and $\underline{\delta}$ satisfies the inequality $0 \le \underline{\delta} \le 1$. Moreover, from the Pythagoras theorem for the right-angled triangle composed of the sides $\underline{r}$, $\underline{r_s}$, and $\underline{\delta}$, it is obtained that:

$$\underline{\delta} = \sqrt{1 - \underline{r_s}^2} \tag{4}$$

According to Eq. (4), for any chosen $\underline{r_s}^* \in [0,1]$ the observed radii $\underline{r_s}$ of spheres cross-sections such that $0 \le \underline{r_s} \le \underline{r_s}^*$ correspond to the sections, distances $\underline{\delta}$ to the center *O* of which satisfy the inequality (see Fig. 3), then:

$$\sqrt{1 - \left(\underline{r_s}^*\right)^2} \le \underline{\delta} \le 1 \tag{5}$$

On the other hand, due to Assumption 4, the normalized length $\underline{\delta}$ of the interval given by Eq. (5) is equal to the probability that the sphere has been cut within this interval. Finally, the probability of $\underline{r_s}$ satisfying the inequality $\underline{r_s} \le \underline{r_s}^*$ is given by the formula:

$$P\left\{\underline{r_s} \le \underline{r_s}^*\right\} = 1 - \sqrt{1 - \left(\underline{r_s}^*\right)^2} \tag{6}$$

Recalling the non-normalized distances, this formula can be presented as a *conditional probability distribution* of r_s under given *r*:

$$P\left\{r_s \le r_s^*\right\} = w\left(r_s^* \middle| r\right) = 1 - \sqrt{1 - \left(\frac{r_s^*}{r}\right)^2} \tag{7}$$

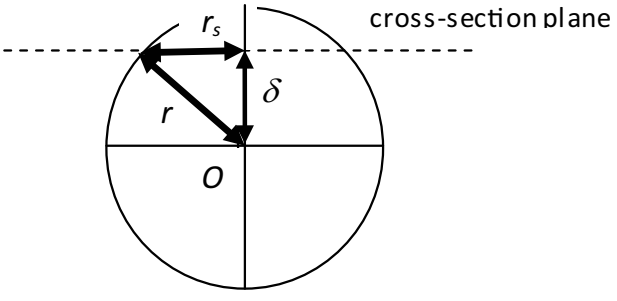

Fig. 3. The scheme of a spherical pore cross-section by horizontal plane.

This function is shown in Fig. 4. However, this is still not what is needed for calculation of *r* when r_s has been measured. This only says that if in an image a large number *N* of quasi-circular cross-sections is observed, then the percentage $p(r^*_s)$ of cross-sections satisfying the condition $\underline{r_s}^* \cdot r \le \underline{r_s} \le r$ is approximated by the formula:

$$P\left(r_s^*\right) \cong \sqrt{1 - \left(\frac{r_s^*}{r}\right)^2} \times 100 \tag{8}$$

For quasi-spherical pores, cross-sections of which satisfy the condition $\underline{r_s}^* \cdot r \le r_s \le r$ for large (i.e., close to 1) $\underline{r_s}^*$, their 3D volumes can be calculated using the approximating formula:

$$V_s \cong \frac{4\pi}{3} \times r_s^3 \tag{9}$$

However, evaluation of pores volumes based on Eq. (9) neglects the fact that some particular cross-sections corresponding to pores of very large *r* may exist among the majority of the other ones satisfying the condition $r_s \cong 0$.

For a given population of selected regular cross-sections in a given image the histograms of their areas S_s, perimeters l_s, shape factors R_s, and equivalent cross-section radii as well as the corresponding mean values and standard deviations can be calculated:

$$r_s = \sqrt{\frac{S_s}{\pi}} \cong 0.564 \times \sqrt{S_s} \tag{10}$$

Similar data can be calculated for volumes given by Eq. (9); however, in this case the validity of the evaluated data is limited by the probability given by Eq. (7).

4. Software

For computer-aided analysis of cross-sections of porous membranes, a specialized program MeMoExplorer™ has been designed. It is an original work dedicated for the Microsoft Windows 10 operating system. The lowest grade of software uses one of the best (and fastest) low-level image processing tool – *Intel Open Computer Vision Library* (OpenCV). It has been written in the most advanced and effective programming C/C++ language, using two development environments:

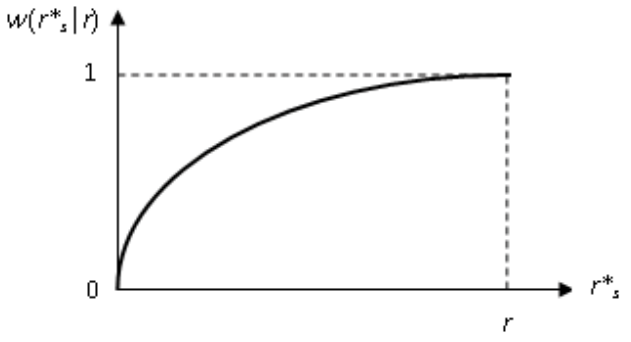

Fig. 4. Conditional probability of $0 \le r_s \le r^*_s$ as a function of r^*_s for given *r*.

Microsoft Visual Studio (Image Processing) and Embarcadero (Borland) RAD Studio (Graphical User Interface). The main task of MeMoExplorer is the full automation of the membrane image processing operations and precise morphometric measurements of pores present in membranes for an objective estimation of their size distribution and preparation of data for a statistical analysis, which can be performed using another software tools (e.g., Excel). A computer analysis of membranes, and more specifically, of their images obtained from the electron microscope, is intended to evaluate the morphological parameters of the porous microstructure and the reproducibility of obtaining these parameters in a complex membrane production process.

The developed program can be easily operated by the end users (technicians and biochemists) and, for this purpose, it is equipped with legible interfaces (see Fig. 5), and offers, in particular, the possibility of automatic:

- acquisition of a series of microscope images of cross-sections of membranes to be analyzed (see Fig. 2);
- acquisition of sets of selected typical images to be used as reference images for classification of the analyzed images into group (see Fig. 5(a), the down right corner);
- segmentation and contouring of cross-sections of pores in the analyzed images;
- classification of the analyzed images based on their similarity to the reference images;
- measurement of areas (S_s) and perimeters (l_s) of the contoured cross-sections of pores;
- selection of objects for analysis;
- calculation of shape factors (R_s) of the cross-sections of pores, division of the cross-sections into the *regular* and *irregular* ones;
- calculation of approximate values of volumes of regular pores;
- calculation of histograms, mean values, and standard deviations of the evaluated parameters in the series of analyzed images; and
- edition of final reports of the analysis.

5. Experiments

Experiments were aimed to prove the possibility of automatic evaluation of selected parameters characterizing the advanced, 3D morphological structure of porous materials on the basis of analysis of SEM images of their 2D cross-sections.

- Starting steps.

For a preliminary selection of images recommended to analysis, a collection of reference images was prepared. For this purpose, 11 sets of exemplary images (10–58 elements in a set), representing various technological types of membranes indicated by an expert, were used. In each image, the pores were automatically contoured. A typical pair of images before and after contouring is shown in Fig. 6. Next, the areas of contours in the image were measured and a histogram $h(S_s)$ of contours size divided into 8 size-classes was calculated. The number of objects analyzed in the image, the maximal, minimal, mean value, and standard deviation of their size were also calculated by the program. A typical screen of the MeMoExplorer™ program containing the results of the discussed data is shown in Fig. 7. In addition, the histograms $g(n_s)$ of the numbers of pores in the size classes and of total image areas covered by them were calculated. This type of histogram is shown in Fig. 8. In the downer part of this histogram, the total areas covered by the cross-sections of the classes are shown.

From all images of any given class, an image containing the highest number of contours, size of which exceeded 300 mm^2 (the most important pore size from the membrane application point of view) was selected.

The selected image was then used as a reference image representative for given (suggested by the examples) similarity classes of porous materials. A typical collection of reference images of 11 similarity classes is shown in Fig. 9 (the numbers assigned to the reference images were also used to denote the classes).

- Classification of the series of images.

Each series of images intended to analysis was assigned to one of the preliminarily distinguished 11 classes; this assignment was based on the highest similarity (minimal absolute distance) of the group of histograms $h(S_s)$ to the histograms of the reference images. The series of images was included into the class, preference histogram of which was the most frequently indicated as the closest one to the histograms of the analyzed images.

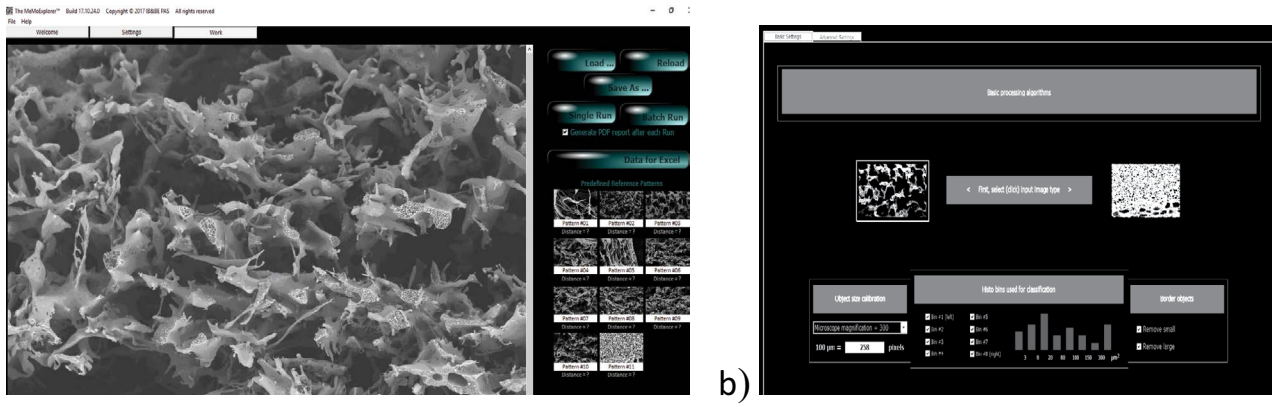

Fig. 5. The screenshots of typical screens of MeMoExplorer™: (a) image acquisition page and (b) objects selection page.

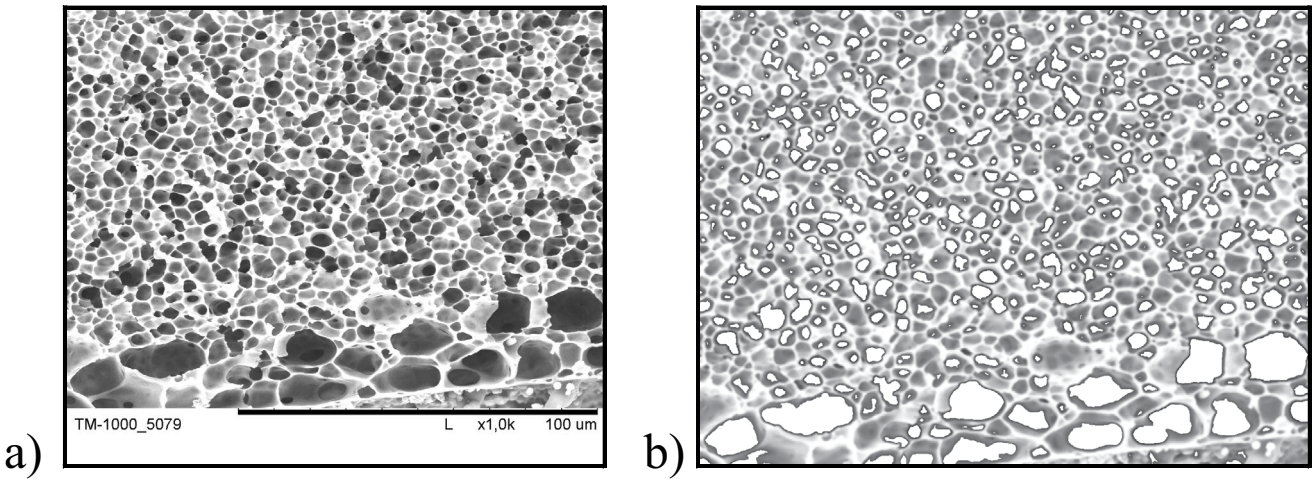

Fig. 6. An image prepared to analysis: (a) original and (b) after automatic contouring.

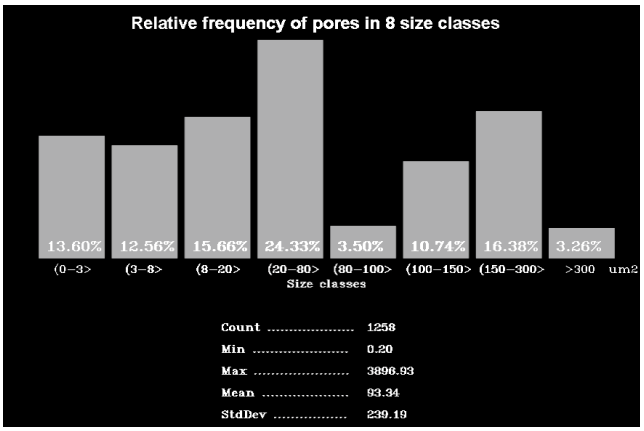

Fig. 7. A typical histogram of the size of pores in a selected image.

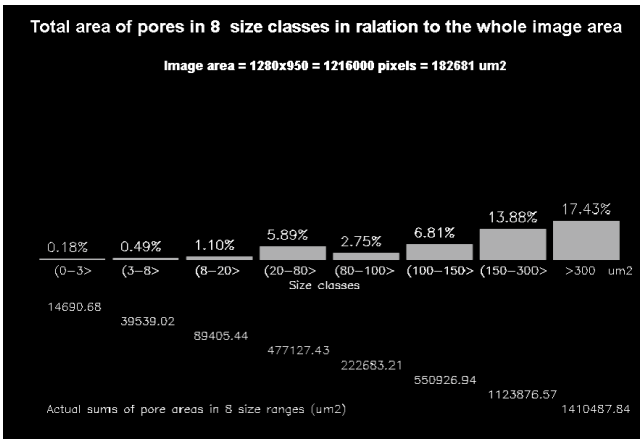

Fig. 8. A distribution of the rate of image area covered by cross-sections of pores in various size-classes.

- Pores' shape regularity assessment.

The classified series of images was next subjected to the assessment of the shape factor R_s of pores (low shape factors corresponded to regular, quasi-circular cross-sections). For each series a histogram $f(R_s)$ of the values of R_s (see Eq. (3)) was calculated. The R_s axis was divided into six intervals according to the indications of an expert. Fig. 10(a) presents a typical histogram of this type, calculated for an image assigned to class #11. It can be noticed, that in this case 84.3% of pores in the analyzed image satisfied the condition $1 \le R_s < 2$. This may be interpreted as a recommendation for image analyzed at the assumption that the majority of pores are quasi-spherical. For comparison, Fig. 10(b) presents a histogram of R_s values calculated in an image assigned to class #3. In this case, only 64.77% of pores were classified as quasi-circular. The mean values of R_s in the compared images were also different: 1.02 in class #11 and 2.27 in class #3.

Objects (cross-sections of pores) accepted for the analysis were next taken into account for evaluation of their approximate volumes V_s using the Eqs. (9) and (10). Fig. 11 shows a histogram $e(V_s)$ of evaluated volumes of pores satisfying the condition of sufficient shape regularity.

Similar calculations were performed in all 11 series of images. However, only one series satisfied the condition of sufficient shape regularity. The rest of series should thus be analyzed using an alternative approach.

The last experiment was aimed to a preliminary proving of the possibility of extraction of additional data useful for 3D porosity analysis from 2D images. For this purpose, the reference image #10 (see Fig. 9) was taken into consideration. Using the "watershed" approach [23], the image was contoured at 100%, 50%, 35%, and 0% of the luminance scale (0–255 levels). The obtained contoured images are shown in Fig. 12. The black spots in images (a)–(d) present the areas of pores' cross-sections, luminance of which does not reach the level of 100%, 50%, etc., of the luminance scale. This is the additional information that provides a relative insight into the 3D structure of pores. A possibility of extraction of this information results in two assumptions: (a) isotropy of porous materials in all three dimensions and (b) statistical independence of morphology characterizing parameters measured in three mutually perpendicular directions. These assumptions can be verified for two admissible directions on the plane of specimens' visualization. The possibility

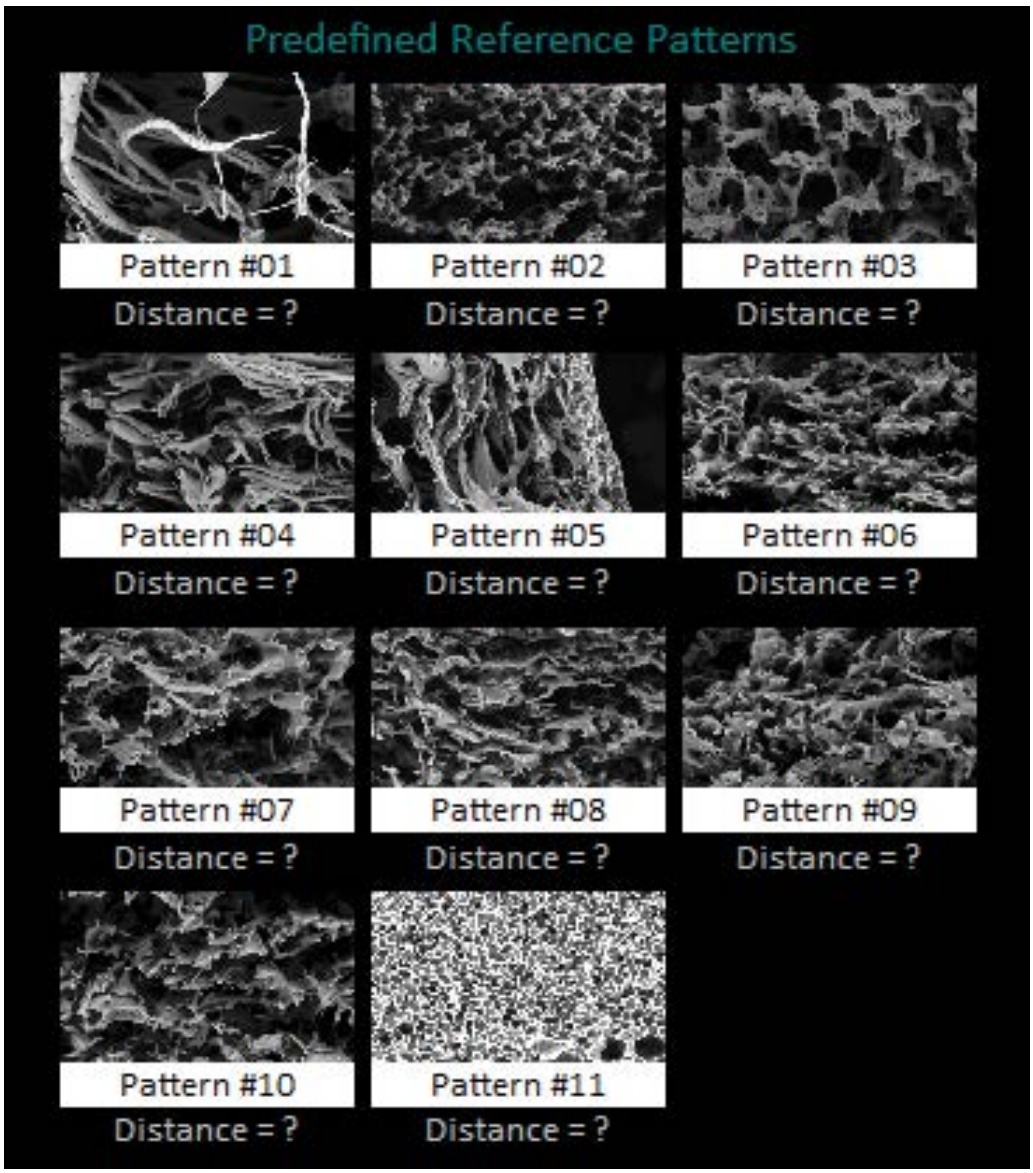

Fig. 9. Reference images used for classification of porous membranes; the numbers of images are also used to denote the classes of membranes.

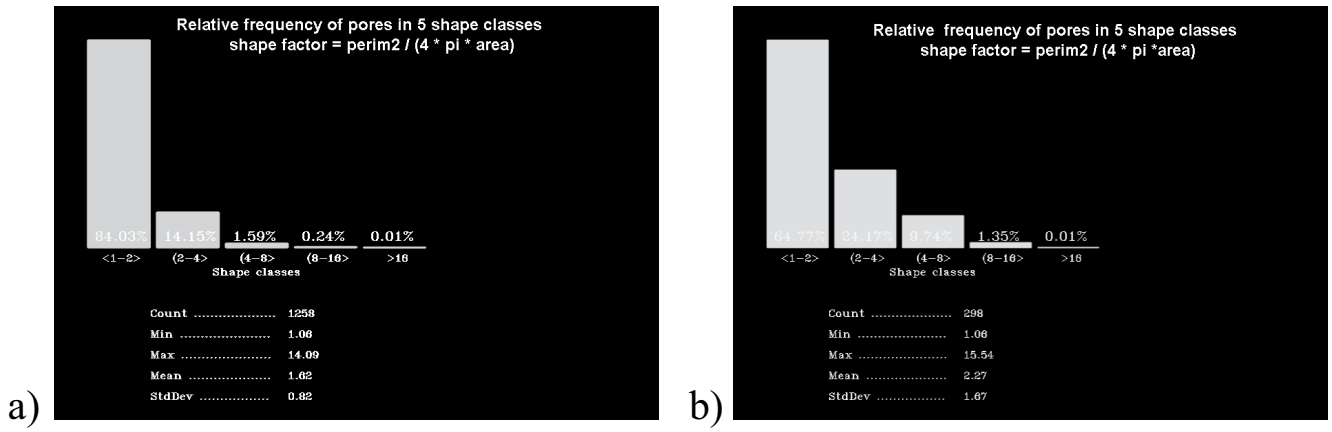

Fig. 10. Typical histograms $f(R_s)$ of shape factor R_s in two images assigned to different classes: (a) class #11 and (b) class #3.

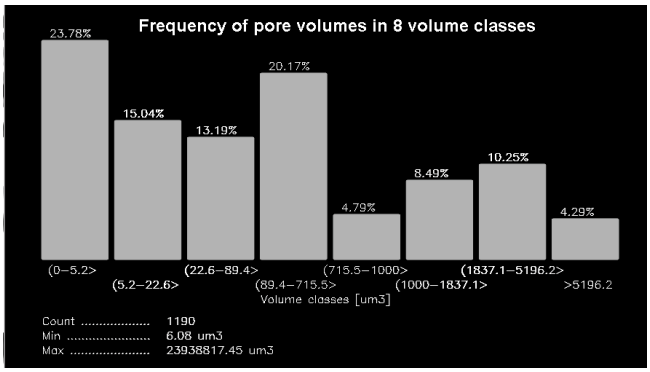

Fig. 11. A histogram $e(V_s)$ of an evaluated volume of regular-shape pores.

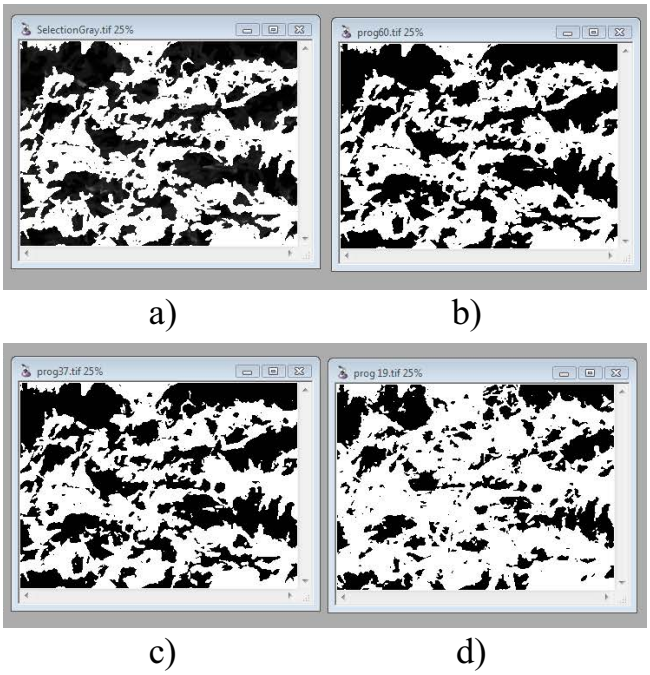

Fig. 12. Cross-sections of a specimen of porous membrane detected at (a) 100%, (b) 50%, (c) 35%, and (d) 0% of luminance-scale level.

of extension of the results of 2D image analysis on the 3D morphological analysis is of particular importance if porous membranes are used as scaffolds for biological cells cultivation. In this case, getting specimens of porous material sliced is practically impossible and statistical extrapolation of observable data seems to be a unique method enabling to 3D porosity characteristics of the materials.

Statistical interpretation of such information will be the topic of a next publication.

6. Conclusions

3D morphological structure of porous materials influences on their biophysical properties and plays an important role in their applications. In particular, it is substantial for porous membranes designed for biological cells cultivation scaffolds. The microscope images of cross-sections of artificial porous membranes provide information about their 2D morphological structure. It has been shown that at specified assumptions concerning regularity of shapes of a sufficiently high percentage of pores, the 3D volume of pores can be evaluated within a controlled statistical error.

For this purpose, a special computer program MeMoExplorer™ can be used. It has also been shown that a deeper computer-aided analysis of the 2D images of cross-sections of porous materials extends the possibility to evaluate the 3D morphological structure of pores of more irregular shape.

This is possible assuming:

- isotropy of porous materials in all three dimensions,
- statistical independence of morphological parameters measured in three mutually perpendicular directions.

The validity of these assumptions can be experimentally proven for two admissible directions on a 2D plane. This possibility seems to be of a great importance for an optimization of the properties of porous materials dedicated to production of scaffolds for cultivation of biological cells.

References

[1] S.J. Hollister, Porous scaffold design for tissue engineering, Nat. Mater., 4 (2005) 518–524.
[2] C.H. Wu, F.K. Lee, S. Suresh Kumar, Q.D. Ling, Y. Chang, Y. Chang, H.C. Wang, H. Chen, D.C. Chen, S.T. Tsu, A. Higuchi, The isolation and differentiation of human adipose-derived stem cells using membrane filtration, Biomaterials, 33 (2012) 8228–8239.
[3] P.Y. Wang, L.R. Clements, H. Thissen, A. Jane, W.B. Tsai, N.H. Voelcker, Screening mesenchymal stem cell attachment and differentiation on porous silicon gradients, Adv. Funct. Mater., 22 (2012) 3414–3423.
[4] A. Higuchi, Q.D. Ling, S.T. Hsu, A. Umezawa, Biomimetic cell culture proteins as extracellular matrices for stem cell differentiation, Chem. Rev., 112 (2012) 4507–4540.
[5] K. Kinasiewicz, K. Dudziński, A. Chwojnowski, A. Weryński, J. Kawiak, Three-dimensional culture of hepatocytes on spongy polyethersulfone membrane developed for cell transplantation, Transplant. Proc., 39 (2007) 2914–2916.
[6] G.C. Engelmayr, M. Cheng, C.J. Bettinger, J.T. Borenstein, R. Langer, L.E. Freed, Accordion-like honeycombs for tissue engineering of cardiac anisotropy, Nat. Mater., 7 (2008) 1003–1010.
[7] H. Lu, N. Kawazoe, T. Kitajima, Y. Myoken, M. Tomita, A. Umezawa, G. Chen, Y. Ito, Spatial immobilization of bone morphogenetic protein-4 in a collagen-PLGA hybrid scaffold for enhanced osteoinductivity, Biomaterials, 33 (2012) 6140–6146.
[8] R. Balena, W. Vidotto da Costaa, J. de Lara Andradea, J.F. Piai, et al., Structural, thermal, optical properties and cytotoxicity of PMMA/ZnO fibers and films: potential application in tissue engineering, Appl. Surf. Sci., 385 (2016) 257–267.
[9] M. Płończak, J. Czubak, G. Hoser, A. Chwojnowski, J. Kawiak, K. Dudziński, K. Czumińska, Repair of articular cartilage defects with cultured chondrocytes on polysulphonic membrane: experimental studies in rabbits, Biocyb. Biomed. Eng., 28 (2008) 87–93.
[10] C.C. Chen, W.C. Wang, S.J. Ding, In vitro physiochemical properties of a biomimetic gelatin/chitosan oligosaccharide/calcium silicate cement, J. Biomed. Mater. Res. B, 95 (2010) 456–465.
[11] Y. Tanaka, H. Yamaoka, S. Nishizawa, S. Nagata, T. Ogasawara, Y. Asawa, Y. Fujihara, T. Takato, K. Hoshi, The optimization of porous polymeric scaffolds for chondrocyte/atelocollagen based tissue-engineered cartilage, Biomaterials, 3 (2010) 4506–4516.
[12] E.C. Ko, Y. Fujihara, T. Ogasawara, Y. Asawa, S. Nishizawa, S. Nagata, S. Nishizawa, S. Nagata, T. Takato, K. Hoshi, BMP-2

embedded atelocollagen scaffold for tissue-engineered cartilage cultured in the medium containing insulin and triiodothyronine – a new protocol for three-dimensional in vitro culture of human chondrocytes, Tissue Eng. Part C, 18 (2012) 374–386.
[13] C.M. Murphy, M.G. Haugh, F.J. O'Brien, The effect of mean pore size on cell attachment, proliferation and migration in collagen-glycosaminoglycan scaffolds for bone tissue engineering, Biomaterials, 31 (2010) 461–466.
[14] S. Nuernberger, N. Cyran, C. Albrecht, H. Redl, V. Vécsei, S. Marlovits, The influence of scaffold architecture on chondrocyte distribution and behavior in matrix associated chondrocyte transplantation grafts, Biomaterials, 32 (2011) 1032–1040.
[15] H. Stenhamre, U. Nannmark, A. Lindahl, P. Gatenholm, M. Brittberg, Influence of pore size on the redifferentiation potential of human articular chondrocytes in poly(urethane urea) scaffolds, J. Tissue Eng. Regener. Med., 5 (2011) 578–588.
[16] S.M. Lien, L.Y. Ko, T.J. Huang, Effect of pore size on ECM secretion and cell growth in gelatin scaffold for articular cartilage tissue engineering, Acta Biomater., 5 (2009) 670–679.
[17] S.H. Oh, I.K. Park, J.M. Kim, J.H. Lee, In vitro and in vivo characteristics of PCL scaffolds with pore size gradient fabricated by a centrifugation method, Biomaterials, 28 (2007) 1664–1671.
[18] M. Kawakami, N. Tomita, Y. Shimada, K. Yamamoto, Y. Tamada, N. Kachi, T. Suguro, Chondrocyte distribution and cartilage regeneration in silk fibroin sponge, Biomed. Mater. Eng., 21 (2011) 53–61.
[19] Z. Qin, L. Hongxu, K. Naoki, Ch. Guoping, Pore size effect of collagen scaffolds on cartilage regeneration, Acta Biomater., 10 (2014) 2005–2013.
[20] A. Chwojnowski, M. Przytulska, D. Wierzbicka, J.L. Kulikowski, C. Wojciechowski, Membrane's porosity evaluation by computer-aided analysis of SEM images, a preliminary study, Biocyb. Biomed. Eng., 32 (2012) 65–75.
[21] J. Adamus, Badanie serca, W. Jakubowski, Ed., Diagnostyka ultradźwiękowa (in Polish), PZWL, Warsaw, 1989, pp. 211–254.
[22] I. Pitas, Digital image processing algorithms and applications, A Wiley-Interscience Publication, New York, 2013, pp. 323–334.
[23] A. Kruk, A. Gadomska-Gajadhur, P. Ruśkowski, A. Chwojnowski, J. Dulnik, L. Synoradzki, Preparation of biodegradable semi-permeable membranes as 3D scaffolds for cell cultures, Desal. Wat. Treat., 64 (2017) 317–323.
[24] K. Dudziński, A. Chwojnowski, M. Gutowska, M. Płończak, J. Czubak, E. Łukowska, C. Wojciechowski, Three dimensional polyethersulphone scaffold for chondrocytes cultivation – the future supportive material for articular cartilage regeneration, Biocyb. Biomed. Eng., 30 (2010) 65–76.